npj | 2D Materials and Applications

www.nature.com/npj2dmaterials

ARTICLE OPEN

Exploring the air stability of $PdSe_2$ via electrical transport measurements and defect calculations

Anna N. Hoffman[1], Yiyi Gu[1,2], Liangbo Liang[3], Jason D. Fowlkes[1,3], Kai Xiao[3] and Philip D. Rack[1,3*]

In this work we investigate the effects of ambient exposure on CVD grown $PdSe_2$ and correlate density functional theory calculations of various physisorption and chemisorption binding energies and band structures to the observed changes in the electrical transport. Pristine $PdSe_2$ is n-type due to intrinsic selenium vacancies, but shows increased p-type conduction and decreased n-type conduction as a function of ambient aging during which various aging mechanisms appear to be operative. Short term aging (<160 h) is ascribed to an activated chemisorption of molecular O_2 at selenium vacancies; first-principles calculations suggest a ~0.85 eV activation energy and adsorption geometries with binding energies varying between 1.3–1.6 eV, in agreement with experimental results. Importantly, this chemisorption is reversible with a low temperature anneal. At long term aging (>430 h), there is a total suppression of n-type conduction, which is attributed to a dissociative adsorption/reaction of the O_2 molecules to atomic O and subsequent PdO_2 formation. XPS confirms the presence of PdO_2 in long term aged flakes. At these extended aging times, the low temperature anneal restores low n-type conduction and suppresses p-type conduction due to the low thermal stability of PdO_2 which, in agreement with XPS measurements, sublimates during the anneal. Thus $PdSe_2$ devices can be processed into device architectures in standard laboratory environments if atmospheric exposure times are limited to on the order of 1 week.

npj 2D Materials and Applications (2019)3:50 ; https://doi.org/10.1038/s41699-019-0132-4

INTRODUCTION

The discovery of atomically thin graphene in 2004 by Novoselov et al. was the catalyst of the 2D materials revolution.[1] In layered materials, such as graphene, hexagonal boron nitride (BN), certain oxides and transition metal dichalcogenides (TMDs), weak Van der Waals forces uniquely keep layers bound together,[2] and thus preparation of atomically thin layers is relatively straightforward via exfoliation from bulk crystals[3–5] or thin film growth.[6,7] Due to its chemical structure, each TMD monolayer has an atomically pristine surface free of dangling bonds and interface traps,[8] which pose a significant issue for silicon and other semiconductor based materials.[9] This allows for vertical scaling in advanced device fabrication with straightforward electrostatics. Processing techniques such as defect engineering,[10] laser irradiation,[11] and plasma exposure[12,13] have been utilized to control material properties and engineer devices with finely tuned properties. Most layered 2D materials have a hexagonal coordination, which promotes atomically flat layers. Recently, 2D materials, which have atoms protruding out-of-plane in a regular corrugated manner, or intralayer "puckering", have become a focus of research due to their interesting properties and added degree of freedom. Puckering has been observed in black phosphorus (BP) among other 2D materials,[14] however air stability has been an ongoing challenge.

Palladium diselenide ($PdSe_2$) has recently been identified as a puckered 2D material, with the additional benefit of a low-symmetry pentagonal structure.[15–17] Structurally, each layer is identical, but there are significant changes in electrical and optical behavior as these layers stack due to changes in symmetry and quantum confinement.[15,18,19] Additionally, $PdSe_2$ is anticipated to be electrically anisotropic; mobility should vary depending on the crystal axis. The most notable and studied layer thickness dependent effect is the transition from an indirect band gap in some bulk TMD materials to a direct band gap in their monolayer counterpart.[18,20] The MoS_2 band gap, for instance, varies from ~1.2 eV in the bulk to ~1.9 eV at the monolayer, while $PdSe_2$ varies from almost no gap (quasi-metallic) to 1.3 eV allowing for unique band gap control.[15,21] This offers a promising path to logic junction devices processed in a single material by patterning various regions with thicker (contact and resistors) and thinner (semiconductor) regions. While some report $PdSe_2$ to be intrinsically ambipolar,[15] as will be demonstrated, we tentatively attribute this behavior to adsorption at surface chalcogen vacancies and find $PdSe_2$ to be intrinsically n-type due to selenium vacancies.

Due to high surface to volume ratio, optoelectronic properties can be dramatically impacted by atmospheric surface adsorbents in 2D materials with strong layer number dependence.[22–24] For this reason it is essential to understand the impact of exposure to ambient, which is often unavoidable during fabrication and characterization processes, on electrical properties. Electrical effects of ambient adsorbents and aging have been studied for MoS_2[2,23,25–29] and WSe_2.[22] Studies on MoS_2 suggest that ambient molecules preferentially adsorb to chalcogen surface vacancies and act as both electron traps and p-type donors.[30] While there is not a consensus on which specific adsorbents contribute to electron suppression and hole doping, most agree that oxygen produces the greatest effect. The effects of water adsorption and long term aging in WSe_2 was recently studied and the enhanced p-type conductivity and n-type suppression was associated with electron transfer to adsorbed water and O_2 molecules and a reduction of the selenium vacancies, respectively.[22] Furthermore, selenides have been shown to be more affected by adsorbed atmospheric species and oxidation effects than sulfides.[16,31]

[1]Department of Materials Science & Engineering, University of Tennessee, Knoxville, TN 37996, USA. [2]Key Laboratory of Photochemical Conversion and Optoelectronic Materials, Technical Institute of Physics and Chemistry, Chinese Academy of Sciences, Beijing 100190, China. [3]Center for Nanophase Materials Sciences, Oak Ridge National Laboratory, Oak Ridge, TN 37831, USA. *email: prack@utk.edu

Published in partnership with FCT NOVA with the support of E-MRS

npj nature partner journals

Previous studies on 2D materials report significant electrical behavior variation after a vacuum or inert atmosphere anneal to drive off adsorbed species such as oxygen and water.[14,16,32] Bartolomeo et al., recently explored the effects of external stimuli such as pressure, and optical and electron irradiation on the electrical properties of exfoliated thick (~25 layer) $PdSe_2$ field effect transistors.[33] Notably they observed a transition from strongly p-type at atmospheric pressure to ambipolar behavior when pumped to $\sim 1 \times 10^{-6}$ Torr. In this work we explore the effects of short term (90 min) ambient exposures and long term (~1000 h) ambient aging and compare atmospheric ambient pressure versus vacuum ($\sim 1 \times 10^{-5}$ Torr) environmental effects on the electrical properties of chemical vapor deposition (CVD) grown multilayer $PdSe_2$; furthermore, we investigate the potential to reverse aging effects through annealing in an inert environment. To rationalize the observed electrical property changes, first-principles density functional theory (DFT) calculations of adsorbed H_2O, O_2 and O on pristine and Se vacancies in single and multilayer $PdSe_2$ were performed.

RESULTS

To investigate the effects of short term ambient exposure on the electrical behavior of $PdSe_2$, a 6 layer $PdSe_2$ FET device was fabricated. Figure 1a shows an optical micrograph and Fig. 1b illustrates a schematic of all devices used in this study. As has been shown previously, $PdSe_2$ FETs annealed at 177 °C in inert gas for 12 min show a strong decrease in p-type conduction, increased n-type conduction, and a negative threshold voltage shift.[16] To confirm this phenomena and investigate the stability of this treatment, Fig. 1c shows the transfer characteristics of a five-layer $PdSe_2$ device measured in air before a 177 °C anneal and the subsequent characteristics measured in air as a function of time after the anneal. We observe the reported strong n-type increase, p-type decrease, and negative threshold voltage shift; however, over a short ambient exposure time there is a strong reversal of these effects. The device shows an increase in the p-type conduction, a gradual decrease in the n-type conduction, and a strong positive threshold voltage shift toward the pre-anneal levels. It should be noted that there is an approximate 5-min delay between the anneal and the first air measurement reported; thus, there is likely some atmospheric exposure effects convoluted in the initial measurement.

To investigate the effect of ambient pressure on the electrical properties, Fig. 1d illustrates a series transfer characteristics of a 13-layer $PdSe_2$ device measured after the 177 °C anneal at various times during an ~22 h, $\sim 1 \times 10^{-5}$ Torr vacuum exposure. It should be noted there is a short period of time (~5 min) between the anneal and the vacuum pump down where the device was exposed to ambient air, first measurement is after 3 min in vacuum. Figure 1c, d, both show the annealed samples have a dominant n-type conduction which we determine to be the pristine behavior of $PdSe_2$. During the vacuum exposure there is a small decrease in the p-type conduction, but at the longer exposure time, p-type conduction approaches the original value. Thus this short term effect (<20 min) could be due to trapped charge injection in the underlying SiO_2 layer caused during the repetitive forward sweep measurement from $-60V_{GS}$ to $+60V_{GS}$.[33] The n-type conduction increases over the first 20 min and remains nearly constant over the next ~22 h. Overall, comparing Fig. 1c, d, dramatic degradation from pristine behavior is observed during atmospheric exposure, but arrested if device is held in vacuum indicating atmospheric adsorbents are the cause. Conversely, Bartolomeo et al., report strong pressure-dependent conduction in bulk-like exfoliated crystals where they observed reversible enhanced p-type conduction at atmospheric pressure and enhanced n-type conduction after an extended (10 h) high-vacuum exposure.[33] Thus, our study which finds no significant pressure-dependent effects is a bit surprising since, as was recently demonstrated in WSe_2,[22] thinner flakes are more susceptible to pressure effects than bulk-like flakes.

Subsequent to the initial short term exposure in Fig. 1, a seven-layer sample was fabricated, annealed, measured, and placed in ambient to be tested after 6, 60, 160, 430 and 840 h of ambient aging. At each aging time, the sample was measured in air, then in vacuum after a 72 h vacuum exposure. Figure 2a illustrates the n-type transfer characteristics measured in air immediately after the anneal, which we assume to be the pristine (time $t = 0$) characteristics. Figure 2a also shows the transfer characteristics of a 6 and 840 h aged sample measured in air and after the 72 h vacuum exposure. The first 6 h of ambient aging clearly suppresses the n-type conduction and significantly increases the p-type conduction. After the 72 h vacuum exposure, n-type conduction increases by a factor of ~4, while the change in p-type conduction is negligible. After 840 h of ambient aging, the device is purely p-type as all n-type conduction has been

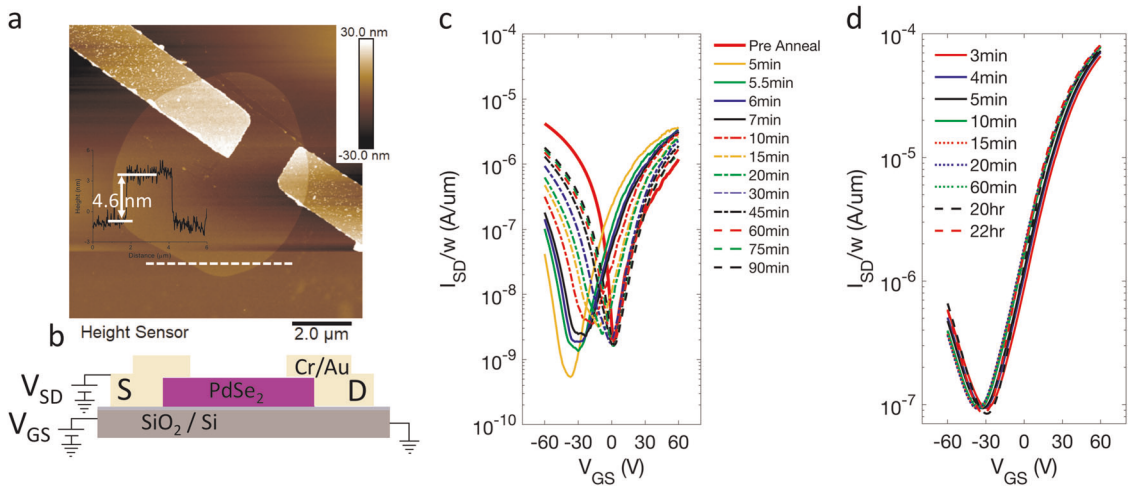

Fig. 1 **a** atomic force micrograph of 7 layer $PdSe_2$ device and **b** schematic of all devices used in this work. **c** transfer characteristics of an as-fabricated five-layer device and subsequent characteristics measured in air as a function of time after an inert, 177 °C −12 min anneal. **d** transfer characteristics of a 13-layer $PdSe_2$ devices after the inert, 177 °C −12 min anneal, measured during various times throughout a ~22 h, $\sim 1 \times 10^{-5}$ Torr vacuum exposure.

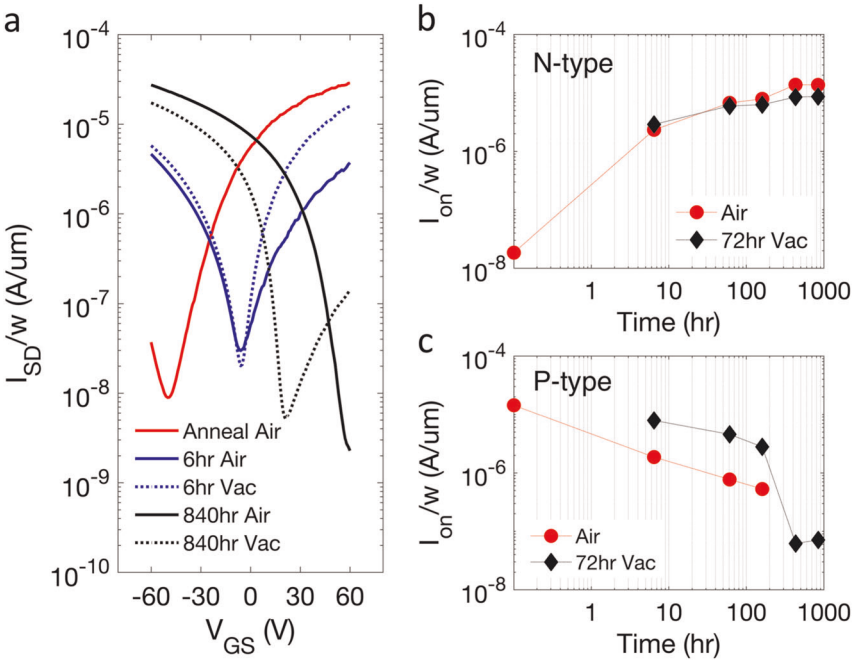

Fig. 2 **a** n-type transfer characteristics measured in air immediately after the anneal which we assume to be the pristine (time $t = 0$) characteristics along with air and post 72 h vacuum exposure characteristics of same device after 6 and 840 h of ambient aging time. **b**, **c** plot the n- and p-type current at ±60 V gate voltage, respectively, versus time in air and after the 72 h vacuum exposure measurements.

suppressed in our gate voltage range. However, after the 72 h vacuum exposure some n-type conduction is recovered. Interestingly, the 840 h aging sample recovers more significantly than the 6 h aging sample (as evidenced by the significant threshold voltage shift) during the vacuum exposure. As will be discussed below, this suggests different aging by-products and in particular that the 6 h aging byproduct has a higher binding energy than the 840 h aging byproduct. Figure 2b, c are plots of the n- and p-type current at ±60 V gate bias versus atmospheric aging time, respectively, measured in air and after the 72 h vacuum exposure (See Fig. S2 for full transfer characteristics). We observe a very clear increase in the p-type conduction and decrease in the n-type conduction over this ambient aging time. Comparing the air and 72 h vacuum exposure measurements, we observe that the change in p-type conduction is negligible (decreases by an average factor of 1.3) and the n-type conduction increases more significantly. For instance, the n-type conduction over the first 160 h increases, on average, by a factor of ~5; at 430 and 840 h the device displays only p-type conduction in air; however, as shown in Fig. 2a, n-type conduction is recovered after vacuum exposure. Thus, the atmospheric aging appears to have a component that is partially reversible via room temperature vacuum exposure.

A complimentary six-layer $PdSe_2$ FET was fabricated and aged along with the sample described above, however this sample was re-annealed prior to each measurement. Figure 3a shows the transfer characteristics of this sample measured in air immediately after each anneal. (See Fig. S3 for transfer characteristics after a 72 h vacuum hold) Clearly the modest aging experienced up to 160 h is largely reversible by the anneal, however some residual degradation to the n-type conduction and enhancement in the p-type conduction remains. Beyond the 160 h measurement, both the n-type and p-type conduction decreases; thus another aging mechanism emerges between the 160 and 430 h aging, which is consistent with the dramatic change in the n-type conduction at 430 h in Fig. 2c. Recently, Bartolomeo et al.[33] studied the hysteresis of multilayer $PdSe_2$ field effect transistors. They attributed the observed hysteresis to charge trapping at $PdSe_2$ defects and in the near interfacial SiO_2 gate region. We also performed hysteresis measurements for some of the aging conditions after the forward measurements made in Figs. 2a and 3 (see supplemental information Fig. S4 for the hysteresis curves). In general, our hysteresis data is similar to those presented in ref. [33]

X-ray photoelectron spectroscopy (XPS) spectra were taken on a pristine $PdSe_2$ sample, samples that were aged in atmosphere for ~120 and ~1000 h, and for reference a $PdSe_2$ sample that was exposed to a 15 s inductively coupled oxygen plasma exposure. Figure 4 illustrates the 3d spin orbit split 5/2 and 3/2 peaks for 3a, Pd and 3b, Se. Kibis et al. recently studied the thermal and plasma oxidation of Pd metal and showed that metallic Pd has 3d 5/2 peak at 335.2 eV, and the typical PdO (Pd^{+2}) peak is at 337 eV.[34] Furthermore, the metastable PdO_2 (Pd^{+4}) exhibit a 3d 5/2 at 338.2 eV. The pristine $PdSe_2$ (Pd^{+4}) peak position of the Pd 3d 5/2 is at 337.4 eV. This is a lower binding energy relative to PdO_2, consistent with Se having a lower electronegativity than O and thus forming a less ionic bond. To confirm the position of the PdO_2 peak, we exposed a $PdSe_2$ sample to oxygen plasma under similar conditions that were found to oxidize a single layer of WSe_2.[13] The ~120 h aged sample has a small Se–O shoulder emerge at ~59 eV and all Pd and Se peaks are shifted ~0.2 eV to lower energy compared to the pristine sample. This peak shift is consistent with a Fermi energy shift to toward the valence band and thus consistent with the observed increase of p-type conduction. At ~1000 h, the S–O peak is still evident, however even more pronounced is the emergence of the PdO_2 peaks at ~338 (5/2) and 343.4 eV (3/2). The Pd and Se peaks are shifted ~0.4 eV to lower energy relative to the pristine sample, which is again consistent with electrical results which show increased p-type behavior at longer ambient aging times. Consistent with Kibis et al, the plasma oxidized PdO_2 3d peaks are ~0.2 eV lower energy compared to the long term ambient aged PdO_2 3d peak.[34] Kibis et al found the PdO_2 oxide from both oxidation methods had low thermal stability over 127 °C, so to support the claim that PdO_2 is forming as $PdSe_2$ samples age in ambient, the ~1000 h aged sample was treated with a 177 °C – 12 min anneal in situ and measured again. Figure 4 shows that after the anneal, oxide peaks

are no longer evident. There is a small peak at 347.5 eV, which is identified as an energy loss peak.[34]

DISCUSSION

To understand the observed change in the $PdSe_2$ electrical properties in response to the annealing process during the atmospheric aging and vacuum exposures, we carried out DFT calculations for the binding energies of adsorbed H_2O and O_2 on pristine single layer $PdSe_2$ as well as several physi- and chemisorbed species at Se vacancy sites for both single and six-layer $PdSe_2$. The computed binding energies and charge transfers (from the $PdSe_2$ to the adsorbents) are summarized in Table 1. Figure 5 compares the associated band structure calculations for the various defect complexes in six-layer $PdSe_2$. Similar calculations for one-layer $PdSe_2$ can be found in supplemental information Fig. S5. Note that the band gap reduction from one-layer (1.36 eV) to six layers (0.27 eV) is slightly overestimated relative to experimentally determined optical band gaps.[15]

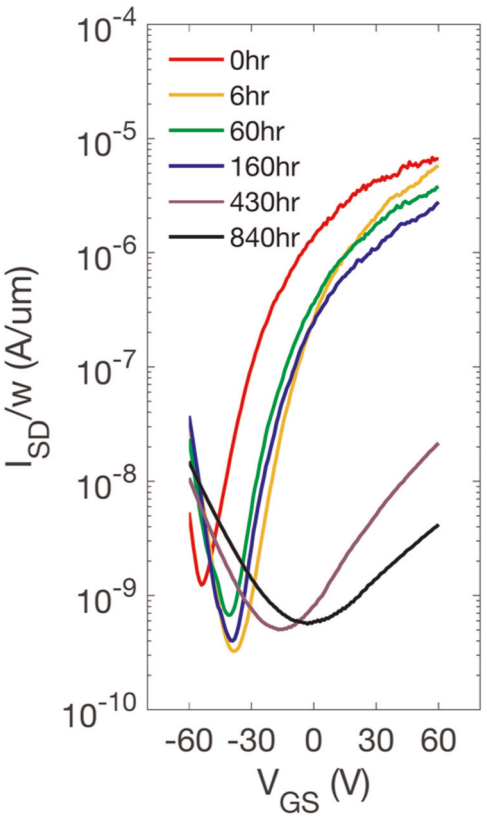

Fig. 3 Transfer characteristics of a six-layer $PdSe_2$ FET measured immediately in air after a 177 °C − 12 min anneal at each of the specified total ambient aging times.

Interestingly, while the O_2 and H_2O physisorbed binding energies and electron transfers per adsorbed molecule from the surface are appreciable, as shown in Fig. 1d, the electrical characteristics of the annealed device is relatively stable after the short air exposure and subsequent 22-h vacuum exposure. The change in $PdSe_2$ electrical properties during ambient air exposure demonstrated in Fig. 1c is thus not attributed to O_2 or H_2O physisorption, which presumably has no energy barrier and would saturate very rapidly upon exposure to ambient. Furthermore, due to the low physisorption binding energies the electrical behavior would be reversible on a much faster time scale than the experimental room temperature vacuum measurements (see residence time plots for O_2 and H_2O physisorption in supplemental information Fig. S6). Physisorption of H_2O to Se vacancies has a higher binding energy, however, Fig. 5d shows that for the six-layer $PdSe_2$, only one of the Se donor levels is degenerate with the conduction band, and thus only a modest Fermi energy shift is expected from this defect complex. Furthermore, this binding energy is also low and thus H_2O would be rapidly desorbed in vacuum, so the relative stability in a room temperature vacuum exposure suggests that this defect complex is not responsible for the observed ambient exposure aging (see H_2O-Se vacancy residence time plot in supplemental information Fig. S6). To estimate the activation energies associated with the observed electrical changes, we correlate the short ambient aging time constant to a simple activated chemisorption process. The estimated time (τ_R) associated with for the n-type conduction to reduce to 1/e (36%) is ~10 min and thus the activation energy can be estimated by $\tau_R = \tau_o \exp\left(\frac{E_a}{kT}\right)$; where τ_o is the vibration frequency of the physisorbed species (~10^{13}/s), E_a is activation energy, k is Boltzmann's constant, and T is temperature. From this expression, an activation energy of ~0.94 eV can be estimated. Furthermore, one can estimate the binding energy of this chemisorbed state by comparing the change in n-type current

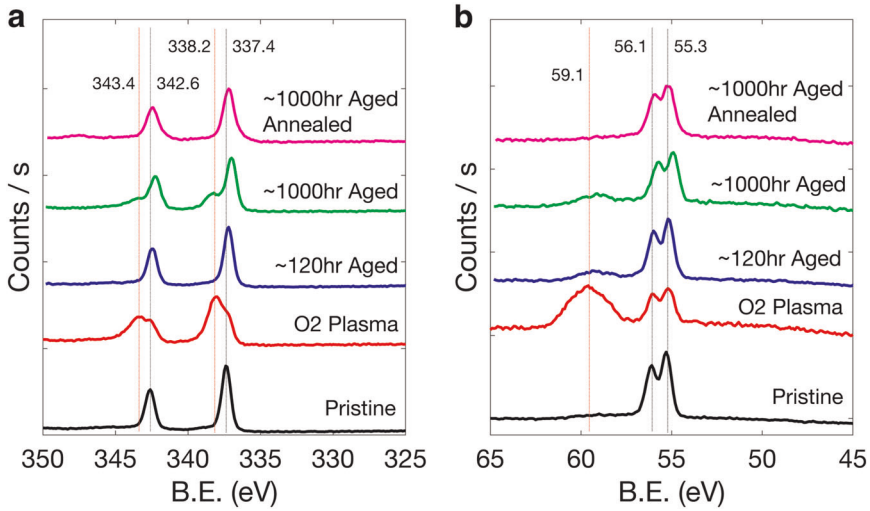

Fig. 4 3d spin orbit split 5/2 and 3/2 peaks for **a** Pd and **b** Se for: a pristine $PdSe_2$ sample; a $PdSe_2$ sample exposed to a 15 s remoted O_2 plasma; $PdSe_2$ samples aged in atmosphere for 120, and 1000 h; and the 1000 h aged sample after a 177 °C − 12 min anneal in situ.

Table 1. Calculated binding energies and charge transfers for various species to pristine $PdSe_2$ and selenium vacancies (V_{Se}) in $PdSe_2$.

	H_2O binding energy (eV)	H_2O charge transfer (e^-)	O_2 binding energy (eV)	O_2 charge transfer (e^-)	O binding energy (eV)	O charge transfer (e^-)
1L	0.13	0.15	0.10	0.06		
1L V_{Se}	0.48	0.51	1.61	1.09	2.10	0.87
6L V_{Se}	0.64	0.46	1.30[a]1.61	1.11	1.99	0.75

[a]rotated 90° relative to 1.61 eV orientation

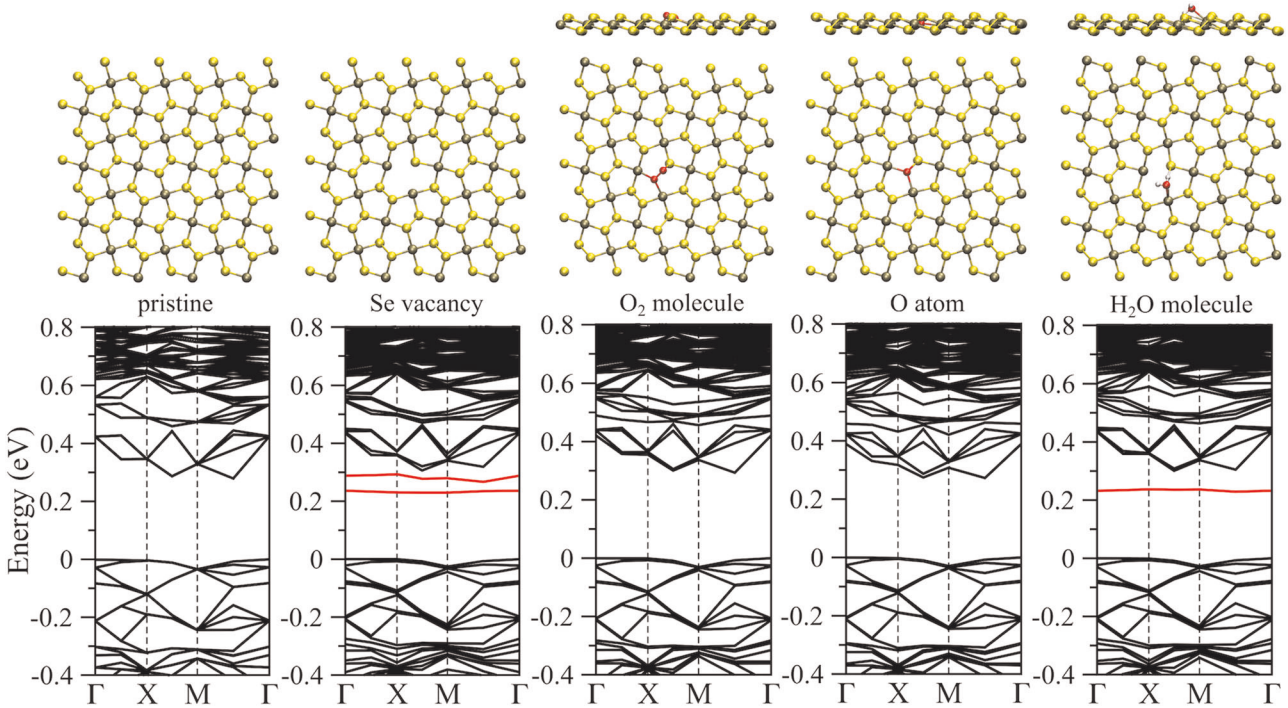

Fig. 5 DFT-calculated electronic band structures of the 4 × 4 supercell of six-layer $PdSe_2$ with **a** no defect, **b** a single selenium vacancy, **c** chemisorption of an O_2 molecule at the vacancy site, **d** chemisorption of an O atom at the vacancy site, and **e** physisorption of a H_2O molecule at the vacancy site. The Fermi level is set at 0 eV, and the in-gap defect bands are highlighted in red colors. The corresponding atomic structure (top and/or side view) is on top of the band structure. Note that only the topmost surface layer of $PdSe_2$ is illustrated here to highlight the interface between the surface and the adsorbates.

after the 72 h vacuum exposure by simple first order desorption kinetics : $\frac{dC}{dt} = \frac{1}{\tau_{des}} C_0 \exp\left(\frac{t}{\tau_{des}}\right)$, where C is concentration, t is time, τ_{des} is the desorption residence time, and C_0 is the concentration at $t = 0$. The estimated binding energy associated with the room temperature change in n-type conduction is 1.07 eV.

Comparing these values to the calculated DFT results suggests that the electrical property changes in response to ambient air exposure can be attributed to an activated chemisorption of O_2 at Se vacancies. While not specifically calculated, one cannot rule out that the some of the chemisorbed O_2 molecules result from the oxygen evolution reaction from adsorbed H_2O catalyzed at the Pd sites associated with the selenium vacancy. As demonstrated in Table 1 and Fig. 5c, molecular O_2 can chemisorb to unsaturated Pd atoms since the O = O double bond can transit to a single bond. While the O_2 molecular chemisorption leaves a defect level near the conduction band edge in single layer $PdSe_2$ (See Fig. S3), both Se vacancy levels are degenerate with the conduction band in the 6 layer material. DFT calculations of the barrier energy associated with the activated chemisorption of physisorbed O_2 to chemisorbed O_2 at the V_{Se} was determined to be about 0.85 eV, which is in good agreement with the estimated value from the time constant of 0.94 eV. The calculated binding energy for the 6 layer chemisorbed O_2 molecule at the Se vacancy is 1.61 eV for the most stable adsorption configuration. The observed room temperature vacuum recovery, however, suggests a slightly lower binding energy of ~1.07 eV; DFT calculations of chemisorbed O_2 molecule rotated 90° yields a slightly lower binding energy of 1.30 eV. This suggests that the computed binding energy of chemisorbed O_2 molecule at the V_{Se} can vary from 1.30 to 1.61 eV depending on the initial orientation of O_2 molecule. In the lower energy case, the reversibility of this short term ambient aging when annealed at 177 °C for 12 min is expected (see 177 °C residence times for 1.1, 1.3, and 1.61 eV in supplemental information Fig. S6) and is experimentally observed in Fig. 3.

The long term aging associated with >160 h ambient exposure is attributed to a dissociative adsorption/reaction of the O_2 molecules to atomic O and subsequent PdO_2 formation, as evidenced by the emergence of PdO_2 in the XPS spectra of a ~1000 h aged sample at ~338 eV.[34,35] PdO_2 formed by plasma oxidation of Pd was found to have low thermal stability >127 °C,[34] and thus should sublime during the 177 °C anneal resulting in damaged surface layer(s) and reduced electron mobility, as seen in the post anneal 430 and 840 h transfer characteristics in Fig. 3. To test this, the ~1000 h aged sample was annealed in situ at

177 °C for 12 min to emulate the device anneal and the XPS spectra re-measured; as demonstrated in Fig. 4, after the anneal the peaks associated with the PdO_2 are gone in agreement with PdO_2 sublimation. An alternative pathway for the dissociation of the molecular O_2 chemisorbed at the Se ($PdSeO_2$) vacancy is the formation of atomic oxygen bound to the Se vacancy (PdSeO). The calculated binding energy of this defect complex in 6 layer $PdSe_2$ is much higher (1.99 eV), and therefore contrary to experiment, this complex would be stable to the prescribed anneal and thus is not believed to be operative. Finally, comparing the >160 h aged device in Fig. 2, the PdO_2 formation continues to enhance the p-type conduction. This behavior is similar to the formation of WO_{3-x} on WSe_2,[13] where the WO_{3-x} layer is electrophilic and traps the donor electrons in the near surface layer region. The apparent low temperature volatility of the PdO_2 is also consistent with the measurement after the 72 hour vacuum exposure, where the purely p-type air measurement recovers only some residual n-type behavior.

In summary, we demonstrate a short term (<160 h) ambient aging effect on the electrical properties of CVD grown $PdSe_2$ where the pristine n-type behaving device exhibits a decrease in n-type conduction and increase in p-type conduction. The aging behavior is arrested when the device is placed in vacuum, confirming that the electrical effect is due to ambient exposure. This short term effect is attributed to activated chemisorption of O_2 at Se vacancy sites, with the DFT-calculated activation energy and binding energy consistent with the experimentally estimated values; the defect complex eliminates the selenium vacancy gap states near the conduction band, which is consistent with the apparent shift in the Fermi energy towards the valence band coinciding with the observed increased p-type conduction. The low binding energy of the molecular chemisorption partially recovers during a long term vacuum exposure and is fully recoverable via a low temperature inert atmosphere anneal. Longer term aging (>430 h) yields a complete suppression of the n-type conduction and a further increase in the p-type conduction. This long term aging is ascribed to a dissociative O_2 chemisorption/reaction where PdO_2 is formed. PdO_2 formation is confirmed via XPS, however the PdO_2 is volatile at low temperatures and thus can be sublimated with a low temperature anneal. The sublimation of the PdO_2 formed on the devices decreases the p-type conduction, and restores some of the n-type conduction, but the conduction is much lower and thus not fully reversible. Notably, the apparent binding energy of the PdO_2 is lower than the chemisorbed O_2 as evidenced by the significant change in the threshold voltage of the long term aged sample after the room temperature vacuum exposure. This study illustrates that if one processes $PdSe_2$ devices in atmospheric conditions any short term aging (~1 week) that occurs is reversible.

METHODS

Growth

The $PdSe_2$ flakes were synthesized by chemical vapor deposition (CVD) method in a one inch tube furnace. The growth was carried out at atmospheric pressure with Ar carrier gas. 20 mg Pd powder (99.95%, Alfa Aesar) was placed in the heating center of the furnace and 1.5 g Se powder (99.9%, Alfa Aesar) was spread on a quartz in the tube. The 300 nm SiO_2/Si substrate was located on the downstream side. The furnace was ramped up to 800 °C within 20 min and held for 10–20 min under an argon gas flow rate of 50–150 sccm (standard cubic centimeter per min). The heating belt controller was set to 350 °C and turned on when the furnace was ramped to 600 °C. It took ~2 min for the heating belt to reach 350 °C. Se powder is placed upstream relative to the Pd powder and the Pd powder region is heated to ~800 °C. The Se is vaporized and reacts with the Pd powder which has a high vapor pressure at its ~760 °C melting temperature.[36–39] The $PdSe_2$ vapor-phase reactants were subsequently transported by the flowing argon gas to the growth region, in which the temperature was around 500–600 °C, thereby inducing the condensation of the 2D $PdSe_2$ crystals on the SiO_2/Si substrate.

Fabrication

Devices were fabricated via electron beam lithography utilizing spin coated Poly(methyl methacrylate) (PMMA) positive resist. Exposure was performed on an FEI 600 Nova equipped with a Raith lithography package. In all, 5 nm Cr/25 nm Au electrodes were electron beam evaporated at 3×10^{-6} Torr at a 0.6 Å/s deposition rate. The pattern was realized by lift off in an acetone bath.

Characterization

Devices were measured in a cryogenic vacuum probe system with a 4200 Keithley semiconductor analyzer. All transfer characteristics presented in the main text are forward sweeps where V_g starts at the most negative value and sweeps toward the most positive value and the curves were collected in 20–30 s (or an average of 4–6 V/s). To study the effect of low temperature annealing, anneals were performed in a nitrogen glove box for 12 min at 177 °C. Samples were typically measured in air, then after ~20 min and subsequent 72 h, $\sim 1 \times 10^{-5}$ Torr vacuum exposure, and then again in air. XPS measurements were performed in a Thermo Electron ESCALAB Xi system with an energy resolution of 0.1 eV. The spot size of the x-ray was approximately 650×650 µm and thus the XPS signal is an average of many individual $PdSe_2$ grains (and background SiO_2). See supplemental information Fig. S1 for optical image of a typical CVD growth of the $PdSe_2$.

Density functional theory calculations

Plane-wave density functional theory (DFT) package VASP was used for first-principles calculations with the projector-augmented-wave (PAW) pseudopotentials and the Perdew-Burke-Ernzerhof (PBE) exchange-correlation functional. In addition, we adopted the van der Waals (vdW) density functional method optPBE-vdW to describe the vdW interactions. To model the $PdSe_2$ surface, single-layer and six-layer $PdSe_2$ structures were built by a periodic slab geometry, where a vacuum separation of about 21 Å in the out-of-plane direction was used to avoid spurious interactions with periodic images. The cutoff energy was set at 400 eV, and a $12 \times 12 \times 1$ k-point sampling was used. All atoms were relaxed until the residual forces were below 0.02 eV/Å, and in-plane lattice constants were also optimized using the method of fixing the total volume (i.e., ISIF = 4 in VASP). Then $4 \times 4 \times 1$ supercell structures of single-layer and six-layer $PdSe_2$ were constructed with a single Se vacancy introduced on the surface to study the adsorption of O_2, O, and H_2O, where the k-point sampling was reduced to $2 \times 2 \times 1$. All the atoms were relaxed until the residual forces below 0.02 eV/Å.

DATA AVAILABILITY

The datasets generated during and/or analyzed during the current study are available from the corresponding author on reasonable request.

Received: 12 August 2019; Accepted: 20 November 2019;
Published online: 13 December 2019

REFERENCES

1. Novoselov, K. S. et al. Electric field effect in atomically thin carbon films. *Science* **306**, 666–669 (2004).
2. Zhu, H. et al. Remote plasma oxidation and atomic layer etching of MoS_2. *ACS Appl. Mater. Interfaces* **8**, 19119–19126 (2016).
3. Zheng, J. et al. High yield exfoliation of two-dimensional chalcogenides using sodium naphthalenide. *Nat. Commun.* **5**, 2995 (2014).
4. Zeng, H., Dai, J., Yao, W., Xiao, D. & Cui, X. Valley polarization in MoS_2 monolayers by optical pumping. *Nat. Nanotechnol.* **7**, 490–493 (2012).
5. Late, D. J., Liu, B., Matte, H. S. S., Rao, C. N. R. & Dravid, V. P. Rapid characterization of ultrathin layers of chalcogenides on SiO_2/Si substrates. *Adv. Funct. Mater.* **22**, 1894–1905 (2012).
6. Zhou, H. et al. Large area growth and electrical properties of p-type WSe_2 atomic layers. *Nano Lett.* **15**, 709–713 (2014).
7. Liu, B. et al. Chemical vapor deposition growth of monolayer WSe_2 with tunable device characteristics and growth mechanism study. *ACS Nano* **9**, 6119–6127 (2015).
8. Liu, W. et al. Role of metal contacts in designing high-performance monolayer n-type WSe_2 field effect transistors. *Nano Lett.* **13**, 1983–1990 (2013).

9. Lai, S. K. Interface trap generation in silicon dioxide when electrons are captured by trapped holes. *J. Appl. Phys.* **54**, 2540–2546 (1983).
10. Stanford, M. G. et al. Focused helium-ion beam irradiation effects on electrical transport properties of few-layer WSe_2: enabling nanoscale direct write homojunctions. *Sci. Rep.* **6**, 27276 (2016).
11. Stanford, M. G. et al. Purification of nanoscale electron-beam-induced platinum deposits via a pulsed laser-induced oxidation reaction. *ACS Appl. Mater. Interfaces* **6**, 21256–21263 (2014).
12. Stanford, M. G. et al. Lithographically patterned metallic conduction in single-layer MoS_2 via plasma processing. *npj 2D Mater. Appl.* **3**, 13 (2019).
13. Hoffman, A. N. et al. Tuning the electrical properties of WSe_2 via O_2 plasma oxidation: towards lateral homojunctions. *2D Mater* **6**, 045024 (2019).
14. Li, L. et al. Black phosphorus field-effect transistors. *Nat. Nanotechnol.* **9**, 372–377 (2014).
15. Oyedele, A. D. et al. $PdSe_2$: pentagonal two-dimensional layers with high air stability for electronics. *J. Am. Chem. Soc.* **139**, 14090–14097 (2017).
16. Chow, W. L. et al. High mobility 2D palladium diselenide field-effect transistors with tunable ambipolar characteristics. *Adv. Mater.* **29**, 1602969 (2017).
17. Puretzky, A. A. et al. Anomalous interlayer vibrations in strongly coupled layered $PdSe_2$. *2D Mater* **5**, 035016 (2018).
18. Mak, K. F., Lee, C., Hone, J., Shan, J. & Heinz, T. F. Atomically thin MoS_2: a new direct-gap semiconductor. *Phys. Rev. Lett.* **105**, 136805 (2010).
19. Lee, C. et al. Anomalous lattice vibrations of single-and few-layer MoS_2. *ACS Nano* **4**, 2695–2700 (2010).
20. Zhao, W. et al. Lattice dynamics in mono-and few-layer sheets of WS_2 and WSe_2. *Nanoscale* **5**, 9677–9683 (2013).
21. Nguyen, G. D. et al. 3D imaging and manipulation of subsurface selenium vacancies in $PdSe_2$. *Phys. Rev. Lett.* **121**, 086101 (2018).
22. Hoffman, A. N. et al. Atmospheric and long-term aging effects on the electrical properties of variable thickness WSe_2 transistors. *ACS Appl. Mater. Interfaces* **10**, 36540–36548 (2018).
23. Park, W. et al. Oxygen environmental and passivation effects on molybdenum disulfide field effect transistors. *Nanotechnology* **24**, 095202 (2013).
24. Zhao, P. et al. Air stable p-doping of WSe_2 by covalent functionalization. *ACS Nano* **8**, 10808–10814 (2014).
25. Giannazzo, F. et al. Ambipolar MoS_2 transistors by nanoscale tailoring of schottky barrier using oxygen plasma functionalization. *ACS Appl. Mater. Interfaces* **9**, 23164–23174 (2017).
26. Nan, H. et al. Strong photoluminescence enhancement of MoS_2 through defect engineering and oxygen bonding. *ACS Nano* **8**, 5738–5745 (2014).
27. Walter, T. N., Kwok, F., Simchi, H., Aldosari, H. M. & Mohney, S. E. Oxidation and oxidative vapor-phase etching of few-layer MoS_2. *J. Vac. Sci. Technol. B* **35**, 021203 (2017).
28. Lee, S. Y. et al. Large work function modulation of monolayer MoS_2 by ambient gases. *ACS Nano* **10**, 6100–6107 (2016).
29. Qiu, H. et al. Electrical characterization of back-gated bi-layer MoS_2 field-effect transistors and the effect of ambient on their performances. *Appl. Phys. Lett.* **100**, 123104 (2012).
30. Ma, D. et al. The role of the intrinsic Se and In vacancies in the interaction of O_2 and H_2O molecules with the InSe monolayer. *Appl. Surf. Sci.* **434**, 215–227 (2018).
31. Jaegermann, W. & Schmeisser, D. Reactivity of layer type transition metal chalcogenides towards oxidation. *Surf. Sci.* **165**, 143–160 (1986).
32. Ovchinnikov, D., Allain, A., Huang, Y. S., Dumcenco, D. & Kis, A. Electrical transport properties of single-layer WS_2. *ACS Nano.* **8**, 8174 (2014).
33. Di Bartolomeo, A. et al. Pressure-tunable ambipolar conduction and hysteresis in thin palladium diselenide field effect transistors. *Adv. Funct. Mater.* **29**, 1902483, https://doi.org/10.1002/adfm.201902483 (2019).
34. Kibis, L. S., Titkov, A. I., Stadnichenko, A. I., Koscheev, S. V. & Boronin, A. I. X-ray photoelectron spectroscopy study of Pd oxidation by RF discharge in oxygen. *Appl. Surf. Sci.* **255**, 9428 (2009).
35. Lupan, O. et al. PdO/PdO_2 functionalized ZnO:Pd films for lower operating temperature H_2 gas sensing. *Nanoscale* **10**, 141107 (2018).
36. Zeng, L.-H. et al. Controlled synthesis of 2D palladium diselenide for sensitive photodetector applications. *Adv. Funct. Mater.* **29**, 1806878 (2019).
37. Wu, D. et al. Highly polarization-sensitive, broadband, self-powered photodetector based on graphene/$PdSe_2$/Germanium heterojunction. *ACS Nano* **13**, 9907–9917 (2019).
38. Luo, L. et al. $PdSe_2$ multilayer on germanium nanocones array with light trapping effect for sensitive infrared photodetector and image sensing application. *Adv. Funct. Mater.* **29**, 1900849 (2019).
39. Okamoto, H. The Pd-Se (palladium-selenium) system. *J. Phase Equilibria* **13**, 69–72 (1992).

ACKNOWLEDGEMENTS

P.D.R., A.N.H., J.D.F and L.L. acknowledge support from the US Department of Energy (DOE) under grant number KC 0403040 ERKCZ01. A.N.H. also acknowledges support from the Center for Materials Processing. Y.G. and K.X. acknowledge support by the U.S. Department of Energy, Office of Science, Basic Energy Sciences, Materials Sciences and Engineering Division. Material growth, device synthesis, DFT calculations, and characterization measurements were conducted at the Center for Nanophase Materials Sciences, which is a DOE Office of Science User Facility. P.D.R. and A.N.H. would like to acknowledge Jonathan Woodward and Harry Meyer for help acquiring the XPS data.

AUTHOR CONTRIBUTIONS

P.D.R. conceived of the experimental plan and managed the project. A.N.H. performed the device fabrication and electrical characterization. Y.G. and K.X. grew 2D $PdSe_2$ crystals; Y.G. performed AFM measurements; A.N.H. with assistance from Jonathan Woodward and Harry Meyer performed X.P.S. measurements; L.L. did the DFT calculations; J.D.F. developed residence time plots. The paper was written through contributions of all authors. All authors have given approval to the final version of the paper.

COMPETING INTERESTS

The authors declare no competing interests.

ADDITIONAL INFORMATION

Supplementary information is available for this paper at https://doi.org/10.1038/s41699-019-0132-4.

Correspondence and requests for materials should be addressed to P.D.R.

Reprints and permission information is available at http://www.nature.com/reprints

Publisher's note Springer Nature remains neutral with regard to jurisdictional claims in published maps and institutional affiliations.